



## Research Article

# Enhancement in air-cooling of lithium-ion battery packs using tapered airflow duct

Vivek K SATHEESH<sup>1,\*</sup>, Navneet KRISHNA<sup>1</sup>, Prakhar Singh KUSHWAH<sup>1</sup>, Ishan GARG<sup>1</sup>,  
Sharmista RAI<sup>1</sup>, Gurumoorthy S HEBBAR<sup>1</sup>, Dileep V NAIR<sup>1</sup>

<sup>1</sup>Department of Mechanical Engineering, CHRIST (Deemed to be University), Bangalore, 560074, India

## ARTICLE INFO

### Article history

Received: 03 November 2022

Revised: 27 February 2023

Accepted: 16 March 2023

### Keywords:

Battery Thermal Management;  
Computational Fluid  
Dynamics; Lithium-ion Battery;  
Temperature Uniformity

## ABSTRACT

Temperature uniformity and peak-temperature reduction of lithium-ion battery packs are critical for adequate battery performance, cycle life, and safety. In air-cooled battery packs that use conventional rectangular ducts for airflow, the insufficient cooling of cells near the duct outlet leads to temperature nonuniformity and a rise in peak temperature. This study proposes a simple method of using a converging, tapered airflow duct to attain temperature uniformity and reduce peak temperature in air-cooled lithium-ion battery packs. The conjugate forced convection heat transfer from the battery pack was investigated using computational fluid dynamics, and the computational model was validated using experimental results for a limiting case. The proposed converging taper provided to the airflow duct reduced the peak temperature rise and improved the temperature uniformity of the batteries. For the conventional duct, the boundary layer development and the increase in air temperature downstream resulted in hotspots on cells near the outlet. In contrast, for the proposed tapered duct, the flow velocity increased downstream, resulting in improved heat dissipation from the cells near the outlet. Furthermore, the study investigated the effects of taper angle, inlet velocity, and heat generation rate on the flow and thermal fields. Notably, with the increase in taper angle, owing to the increase in turbulent heat transfer near the exit, the location of peak temperature shifted from the exit region to the central region of the battery pack. The taper-induced improvement in cooling was evident over the entire range of inlet velocities and heat generation rates investigated in the study. The peak temperature rise and maximum temperature difference of the battery pack were reduced by up to 20% and 19%, respectively. The proposed method, being effective and simple, could find its application in the cooling arrangements for battery packs in electric vehicles.

**Cite this article as:** Satheesh VK, Krishna N, Kushwah PS, Garg I, Rai S, Hebbar GS, Nair DV. Enhancement in air-cooling of lithium-ion battery packs using tapered airflow duct. J Ther Eng 2024;10(2):375–385.

### \*Corresponding author.

\*E-mail address: [vivek.satheesh30@gmail.com](mailto:vivek.satheesh30@gmail.com)

*This paper was recommended for publication in revised form by Editor-in-Chief Ahmet Selim Dalkılıç*



## INTRODUCTION

Electric vehicles commonly use lithium-ion battery packs for energy storage due to their high energy density, low self-discharge rate, and long cycle life [1]. The electrochemical reactions during the charging and discharging of lithium battery cells produce a significant amount of heat, which could lead to temperature rise and adversely affect the batteries' lifespan, safety, and power output [2]. The safe allowable temperature range for lithium-ion batteries is 25–40 °C, and the temperatures outside of this range directly affect the efficiency and safety of the battery pack [3]. Furthermore, for every degree Celsius temperature increase from the ideal operating range, the life of a lithium-ion battery cell is shortened by ~8 weeks. Maintaining the pack within a suitable temperature range and reducing the temperature differential between the cells are imperative for appropriate battery pack performance [4]. Thus, thermal management of the battery pack is crucial for its effective and reliable operation [5].

Air cooling is a commonly used battery cooling method because of its simplicity, cost-effectiveness, minimal additional components, and minimal space requirements [6]. The conventional battery air-cooling system uses unidirectional airflow from the inlet to the outlet of the pack [7]. The air is heated as it flows from the inlet to the outlet, and the resulting increase in air temperature reduces the heat transfer coefficient downstream. As a consequence, the cells located upstream (near the air inlet) are typically at lower temperatures compared to the cells located downstream (near the air outlet) [8]. This results in thermal non-uniformity across the cells and inadequate cooling of cells located near the outlet.

### Literature Review

Several studies attempted to improve the heat transfer performance in air-cooled lithium-ion battery packs. Some of these studies utilized variation in the flow direction to attain temperature uniformity within the cells. For example, Mahamud and Park [9] used reciprocating airflow, where the airflow reversed its direction after regular time intervals, to reduce the cell temperature difference by up to 72%. The reciprocating flow resulted in heat redistribution and disruption of the thermal boundary layers on the cells, leading to a reduction in the peak temperature of the cells. Li et al. [10] investigated a U-type air-cooling battery thermal management system with multiple airflow configurations; they identified a design with three inlet and outlet manifolds for effective heat transfer performance. Shun-Bo et al. [11] demonstrated that the inlet air velocity and position of the outlet significantly influence the cooling efficiency of the battery pack. Yu et al. [8] employed two independent air ducts to enhance thermal performance; one was a conventional cooling duct, and the other used jet cooling to remove accumulated heat from the cells in the middle of the pack. Na et al. [2] explored the use of two independent air channels formed by dividing the original flow channel

using a diathermanous partition. The reversed layered airflow in the channels significantly improved the cooling performance compared to unidirectional flow.

A few studies on air-cooled battery packs used modification in flow paths for improved airflow distribution. Wang et al. [12] investigated a battery thermal management system that used spoilers to alter the direction of airflow; the method could lower the maximum temperature and increase temperature uniformity. The study discussed the impact of length, shape, and the number of spoilers on cooling performance. Ibrahim et al. [13] considered a rhombic arrangement of battery cells and examined the impact of the size of the inlet and outlet ducts on cooling at various inlet air velocities. The peak and average temperatures reduced with an increase in air velocity. Park [14] proposed tapered manifolds and pressure relief vents to attain uniform distribution of airflow in the coolant passages. In another design, tilting the battery pack to form a wedge-shaped runner resulted in airflow distribution conducive to thermal uniformity across the cells [15]. A similar configuration of wedge-shaped intake and exit plenum was studied by Saw et al. [16]. Lu et al. [17] used irregular airflow paths in densely packed lithium-ion cells to attain thermal uniformity and eliminate hotspots. Other examples of flow path modification to improve the cooling performance includes using a “double U” type duct [18] and air distribution pipes [19].

Some studies explored the changes in the arrangement and orientation of the cells in air-cooled battery packs. Yang et al. [20] investigated axial airflow cooling of cylindrical lithium-ion batteries. They observed the effects of air flux and radial intervals between the cells on the temperature distribution in the cells. Fan et al. [21] studied aligned, staggered, and cross arrangements of air-cooled cells and concluded that cooling efficiency is superior in the aligned arrangement. Singh et al. [22] discussed the impact of cell arrangement on heat transfer using air-cooling in combination with phase change material. At higher air velocities, the heat transfer performance was superior with a diamond cell arrangement than a square arrangement. Ibrahim et al. [23] numerically studied the air-cooling of a unique triangular battery pack configuration, considering the effect of the relative positions of an inlet and the two outlets on the cooling of the battery pack [23]. The study observed that increasing the air velocity reduced the peak cell temperature. Alharbi et al. [24] evaluated a battery pack with three configurations—lozenge, rectangular, and triangular—and found that the triangular arrangement resulted in the pack's lowest mean and maximum temperatures [24]. Simulation-based studies have been extensively used [25] for investigating flows [26], and existing experimental data can be used to validate the numerical models [27]. In a simulation-based research, Hai et al. [28] studied the heat transfer of a battery pack with 16 cells and evaluated the aligned arrangement versus the non-aligned arrangement. The aligned arrangement had a lower peak temperature, and the peak temperature decreased with an increase in air velocity. In other

related studies, design modifications using agents like baffle plates [29], spoilers [30], bionic surfaces [31], and fins [32] exhibited enhanced heat dissipation.

**Problem Definition and Objectives**

The studies discussed in the literature review reiterate the importance of (i) reducing the peak temperature of the battery pack and (ii) attaining temperature uniformity within the cells of the battery pack. Compared to liquid cooling, air cooling has several benefits, including a simple structural design, lower costs, light weight, ease of maintenance, high durability, convenience in replacing a single cell, and reduced parasitic power consumption [33]. Hence, any intricate design modification that negates these advantages may not be practical in real-world applications.

The present study proposes and explores the use of a simple tapered, converging, unidirectional airflow duct to enhance the cooling performance in lithium-ion battery packs. In the thermal management of battery packs, the major drawback of conventional unidirectional airflow ducts is that the downstream cells are not adequately cooled due to the increase in air temperature downstream. The downstream heat transfer coefficient decreases as the downstream air temperature increases. As a result, the cell temperature increases from the inlet to the exit, leading to temperature nonuniformity, and hotspots are observed on the cells near the exit. However, by replacing the conventional non-tapered duct with a converging duct, the flow velocity increases downstream, enhancing the local heat transfer from the cells downstream. The proposed simple method can achieve (i) a reduction in peak temperature in cells near the exit and (ii) attainment of temperature uniformity across the cells without adding significant complexity to the overall design.

The study considers air cooling of a battery pack of 18650 lithium-ion cells using non-tapered and tapered ducts. The objectives of the study are as follows:

- (i) Develop and validate a computational model to investigate air cooling of lithium-ion battery packs.
- (ii) Compare the flow and thermal fields of non-tapered and tapered ducts and evaluate the reduction in peak temperature and improvement in temperature uniformity attained using the proposed tapered duct.
- (iii) Discuss the cooling performance of the ducts considering different taper angles, inlet velocities, and heat generation rates.

**NUMERICAL MODEL**

**Computational Domain**

The battery module was a stack of 18650 lithium-ion cells, which were cylindrical with a diameter ( $D$ ) of 18 mm and a height of 65 mm. The cells were arranged in two rows having twelve cells in each row (the arrangement is adopted from [34]). Two models were considered for the comparative numerical analysis: (i) the conventional non-tapered

duct (Figure 1) and the proposed tapered duct (Figure 2). The cells and the air within the duct constituted the computational domain. The rectangular duct inlet had a width ( $W$ ) equaling 62 mm and a height ( $H$ ) equaling 180 mm. The duct had a length ( $L$ ) of 247 mm along the  $z$ -direction

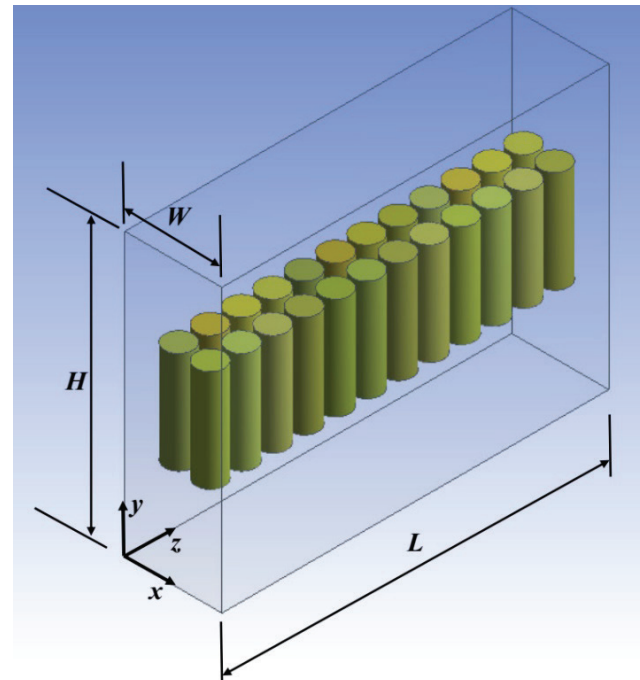


**Figure 1.** Computational domain and coordinate system for the lithium-ion cells with the conventional non-tapered duct.

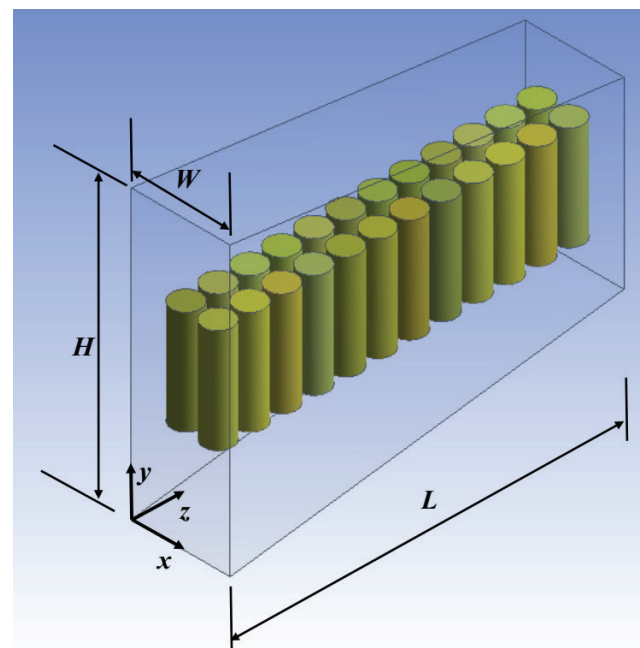


**Figure 2.** Computational domain and coordinate system for the lithium-ion cells with the proposed tapered duct.

(the coordinate system is marked in Figures 1 and 2). The battery module was placed symmetrically inside the airflow duct. Within the battery module, the cells were spaced 2 mm apart.

### Method of Solution

The study considered uniform heat generation in each cell in the battery pack. The cooling air was treated as incompressible. The relevant governing equations are as follows.

Energy equation (cells):

$$\frac{\partial}{\partial x} \left( k_{cell,x} \frac{\partial T}{\partial x} \right) + \frac{\partial}{\partial y} \left( k_{cell,y} \frac{\partial T}{\partial y} \right) + \frac{\partial}{\partial z} \left( k_{cell,z} \frac{\partial T}{\partial z} \right) + q_{gen} = \rho_{cell} c_{cell} \frac{\partial T}{\partial t} \quad (1)$$

Continuity equation:

$$\rho_{air} \nabla \cdot (\vec{V}) = 0 \quad (2)$$

Momentum equation:

$$\rho_{air} \frac{\partial \vec{V}}{\partial t} + \rho_{air} \nabla \cdot (\vec{V} \vec{V}) = -\nabla p + \mu \nabla^2 \vec{V} \quad (3)$$

Energy equation (air):

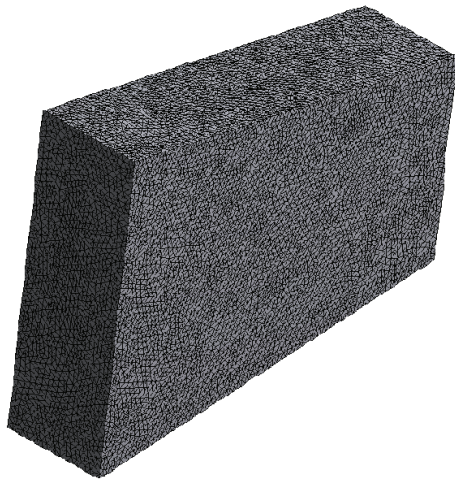
$$\rho_{air} c_{air} \frac{\partial T}{\partial t} + \rho_{air} c_{air} \nabla \cdot (\vec{V} T) = k_{air} \nabla^2 T \quad (4)$$

ANSYS FLUENT 19.2 solver was used for the numerical solution. The finite-volume method is employed in the solver. For the cylindrical cell, the values of Reynolds number ( $Re = \rho U D / \mu$ ) encountered in the study was above 675, and hence the flow was deemed turbulent [35]. The

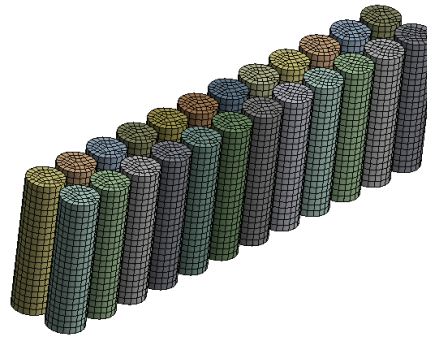
study used the standard *k-epsilon* turbulence model [36]. The solution followed the SIMPLE algorithm. The discretization scheme was second-order for pressure and second-order upwind for momentum and energy equations. The first-order implicit scheme was used for time-stepping. At convergence, the scaled residuals [37] were less than  $10^{-3}$  for the continuity equation,  $10^{-4}$  for the momentum equation, and  $10^{-8}$  for the energy equation.

The thermophysical properties of the cells were adopted from [34] as follows:  $\rho_{cell} = 2478 \text{ kg/m}^3$ ,  $c_{cell} = 806 \text{ J/kgK}$ ,  $k_{cell,x} = k_{cell,z} = 1.3 \text{ W/mK}$ , and  $k_{cell,y} = 14.15 \text{ W/mK}$ . The velocity was specified at the inlet of the duct, and the air temperature at the inlet was 298 K. No-slip boundary condition was imposed at the walls of the duct and the cells. Equality of temperature and continuity of heat flux were imposed at the solid–fluid interface on the cell walls. The walls of the duct were adiabatic. The pressure was atmospheric at the outlet of the duct. Heat generation was applied as a source term within the cells. The cells were at an initial temperature of 298 K. Considering the 3C discharge of the batteries, the transient simulations were carried out for 1200 s, with a time step of 1 s.

Figure 3 shows the meshed computational domain. The selected mesh had a total number of  $6.8 \times 10^5$  elements. For  $q_{gen} = 50000 \text{ W/m}^3$ , inlet velocity = 1 m/s, and taper angle =  $15^\circ$ , the selected mesh predicted a peak temperature of 306.6 K within the cells. A finer mesh with  $9.6 \times 10^5$  elements predicted a peak temperature of 306.5 K within the cells, with other conditions remaining the same. Thus, between the selected mesh and the finer mesh, the difference in the prediction of peak temperature is marginal ( $\sim 0.1 \text{ K}$ ), thereby demonstrating grid independence.



(a) Meshed domain within the duct



(b) Meshed domain within the cells

Figure 3. Meshed computational domain.

## RESULTS AND DISCUSSION

The air-cooling of the pack comprising 24 lithium-ion batteries (18650-type cells) arranged in two rows was simulated using ANSYS FLUENT 19.2 solver. This section presents the validation of the numerical model and discusses the effect of tapered duct design on the temperature distribution of the battery pack. Further, the effects of taper angle, inlet air velocity, and heat generation rate on the cooling of the battery pack are discussed.

### Validation

A limiting case validation was performed by comparing the results of the present numerical simulation with the experimental results of Stanescu et al. [38] for free-stream cross-flow forced convection from an array of heated cylinders. The experiments in [38] used a bundle of cylindrical heaters mounted between two wooden walls. The heating element within each cylinder uniformly distributed the heat throughout the array. We carried out simulations for the arrangement in [38] having  $S/D$  ratios of 0.25, 0.5, and 0.75 (23 cylinders, 16 cylinders, and 14 cylinders, respectively); here,  $S$  is the cylinder-to-cylinder spacing, and  $D$  is the cylinder diameter, as defined in [38]. The experimental results were for a steady state. Hence, for comparison, the transient simulations were forwarded in time until the cylinder temperatures reached a steady state. The cylinder temperatures were steady after a flow time of 700 s in the numerical simulations. Figure 4 shows the comparison between the numerical results and the experimental results. The definition of  $S/D$ , Reynolds number ( $Re$ ), and dimensionless overall thermal conductance ( $\bar{q}$ ) follow from [38]. The results predicted by the numerical solver closely

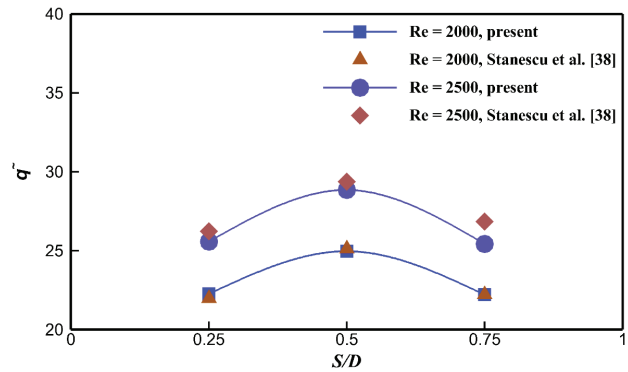


**Figure 4.** Comparison of present numerical results with the experimental results of Stanescu et al. [38].

matched the experimental results with a maximum variation of 6% and an average variation of 2%.

### Effect of Proposed Tapered Duct Design

This section compares the thermal performance of the conventional non-tapered duct with the proposed tapered duct to understand the influence of the taper on heat transfer in the air-cooled battery thermal management system. Figure 5(a) gives the temperature rise on the surface of the lithium-ion cells (i.e., the difference between cell temperature and ambient temperature) for the conventional duct. The temperature contours reveal that the cells downstream and close to the outlet are at significantly higher temperatures than those upstream. This is due to a reduced local heat transfer coefficient owing to the increased air temperature downstream. Figure 5(b) shows the temperature rise within the lithium-ion cells at mid-height of the duct

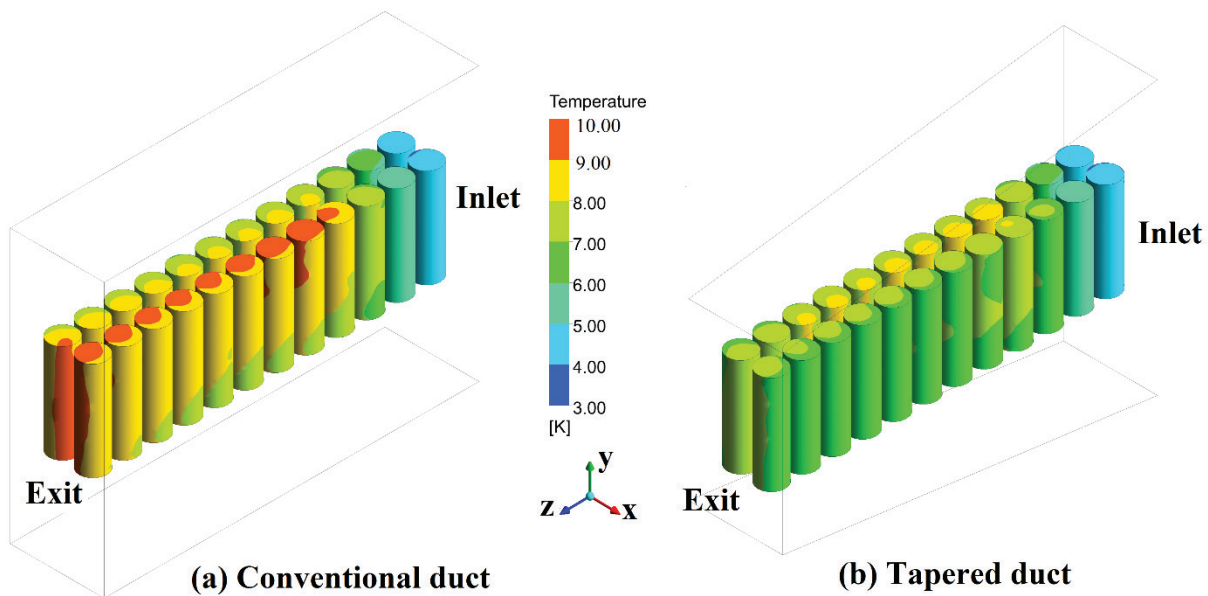


**Figure 5.** Temperature rise on the cell surface for inlet velocity of 1 m/s,  $q_{gen} = 50000 \text{ W/m}^3$ , and taper angle =  $15^\circ$ .

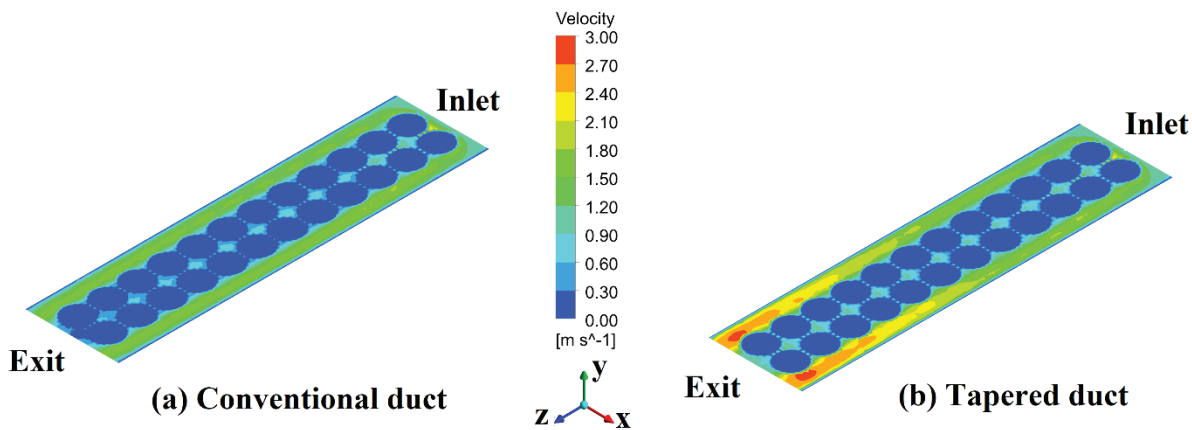


**Figure 6.** Velocity distribution atop the cell surface for inlet velocity of 1 m/s,  $q_{gen} = 50000 \text{ W/m}^3$ , and taper angle =  $15^\circ$ .

for the proposed tapered design with a taper angle of  $15^\circ$ . The results reveal a significant reduction in (i) the peak temperature on the cell surface and (ii) the temperature of the cells near the outlet for the proposed tapered duct. The peak temperature rise for the proposed tapered duct is 11.7% lower than that for the conventional duct.

For the tapered duct, the reduction in cross-sectional area downstream results in increased flow velocities downstream. The increased flow velocities downstream improve the local heat transfer coefficient downstream. Thus, in the case of the converging tapered duct, the effect of reduction in local heat transfer coefficient downstream due to the increase in air temperature is compensated by the effect of an increase in local heat transfer coefficient resulting from the increased flow velocities. The above-mentioned reason explains the improved cooling performance of the proposed tapered duct when compared to the non-tapered duct. For further clarity, the velocity contours atop the cell surface within the duct channel are presented in Figure 6 (a) and (b) for the conventional duct and the tapered duct, respectively. A substantial increase in the flow velocities downstream is evident for the tapered duct.

### Parametric Study

The parametric study investigated the effect of taper angle, inlet velocity, and heat generation rate on thermal performance.

#### Taper angle

The taper angle was varied from  $10^\circ$  to  $25^\circ$  to study its effect on the cooling performance. Furthermore, the results for different taper angles were compared with those for the conventional duct model. The taper angle was varied by varying the outlet cross-section (i.e., by varying the height of the duct outlet) while maintaining the inlet cross-section and inlet velocity unchanged. Hence, the airflow rate was maintained the same for all the models.

The following are three major observations from the study:

- (i) Figure 7 shows the velocity contours at mid-channel height for taper angles of  $10^\circ$ ,  $20^\circ$ , and  $25^\circ$ . Assisted by the taper, the velocity increases towards the outlet of the duct, and the extent of the increase in velocity is more significant for higher taper angles. For taper angle =  $10^\circ$ , the peak velocity near the outlet is  $\sim 1.5 \text{ m/s}$ ; this peak velocity increases to  $\sim 3 \text{ m/s}$  for a  $20^\circ$  taper angle; a further increase in taper angle to  $25^\circ$  results in a maximum velocity of  $\sim 4 \text{ m/s}$  near the exit.
- (ii) Figure 8 presents the contours of temperature rise across the surface of the cells for taper angles of  $10^\circ$  and  $25^\circ$ . Assisted by the increase in flow velocity and the associated improvement in the local heat transfer coefficient downstream, the temperature of the cells located near the outlet drops with an increase in taper angle. Furthermore, the peak temperature rise of the  $25^\circ$  taper angle is 8% lower than that of the  $10^\circ$  taper angle.
- (iii) Figure 8 reveals that, especially for large taper angles, the location of peak cell temperature shifts from the outlet region of the duct to the central region. For higher taper angles, the flow velocities are significantly higher downstream, increasing turbulence near the duct outlet. Consequently, the local heat transfer in the downstream region enhanced considerably. This explains the re-location of peak temperature from the outlet region to the central region of the duct for higher taper angles.

#### Inlet velocity

To understand the influence of inlet velocity on the thermal performance enhancement resulting from the tapered duct, simulations were carried out on the tapered duct and the conventional duct with inlet velocities ranging from 0.6 m/s to 1.4 m/s. Introducing a tapered duct reduces the hotspots in cells near the outlet for the range of inlet velocities considered in the study. For an inlet velocity of 0.6 m/s, the temperature rise in the cells at mid-height of the battery pack for the conventional duct and the tapered duct (taper

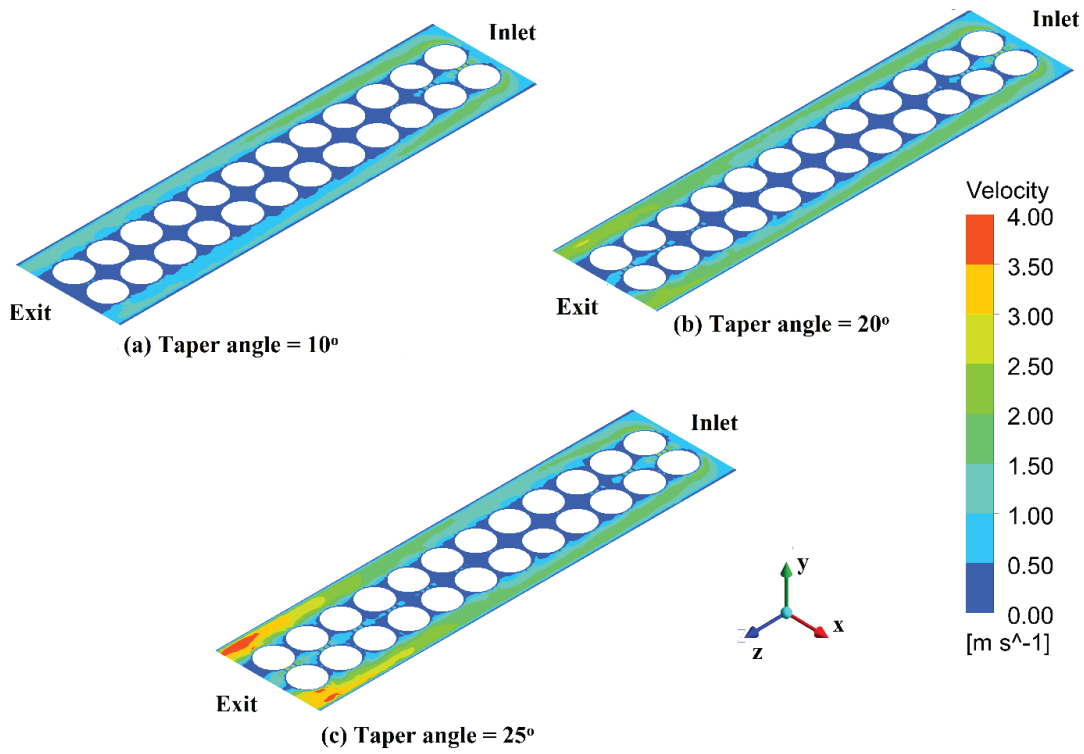


Figure 7. Velocity distribution at mid-channel height for inlet velocity of 0.8 m/s and  $q_{gen} = 50000 \text{ W/m}^3$ .

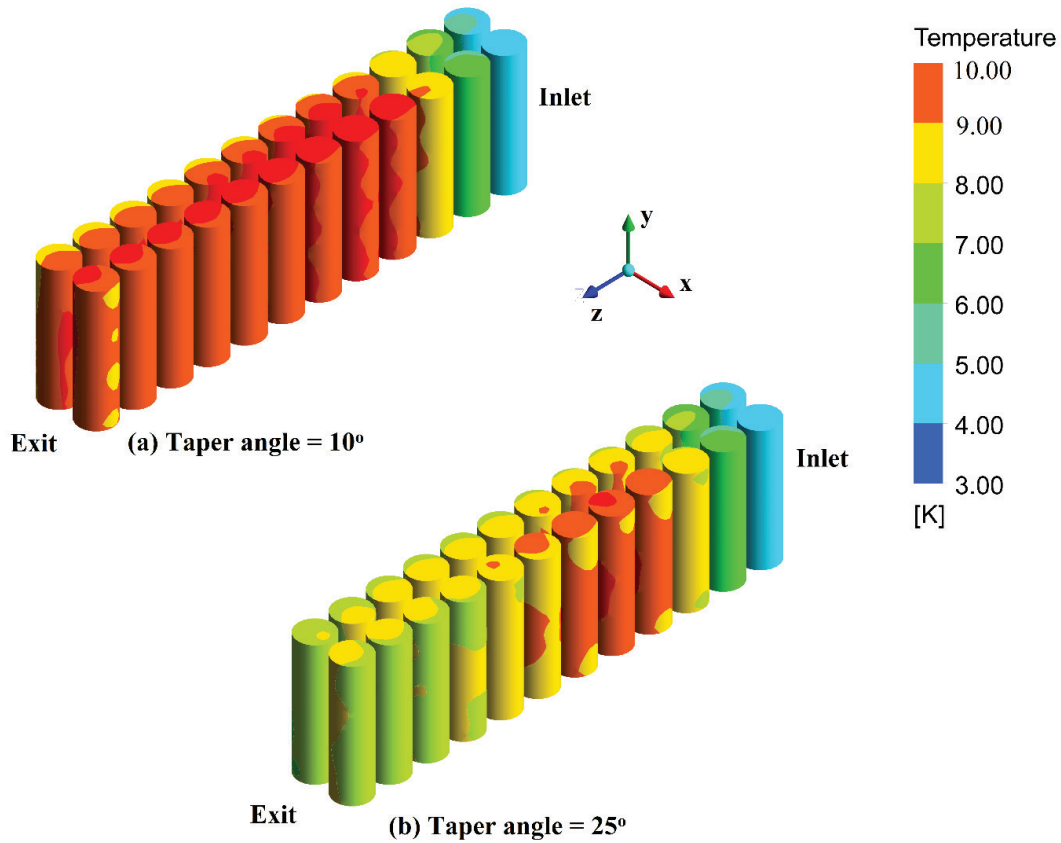


Figure 8. Temperature rise on the cell surface for inlet velocity of 0.8 m/s and  $q_{gen} = 50000 \text{ W/m}^3$ .

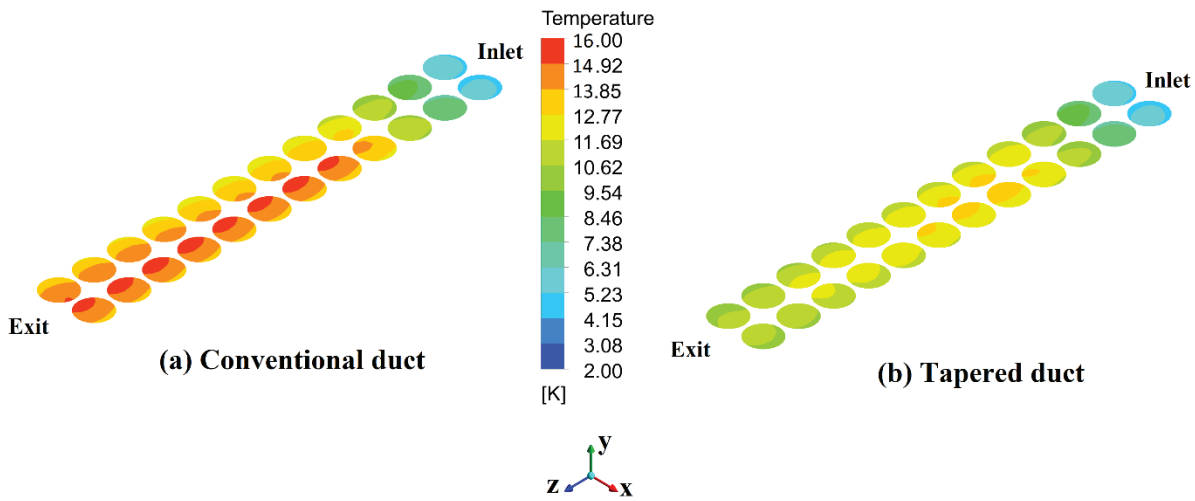


Figure 9. Temperature rise at mid-height of the battery pack for inlet velocity of 0.6 m/s,  $q_{gen} = 50000 \text{ W/m}^3$ , and taper angle = 15°.

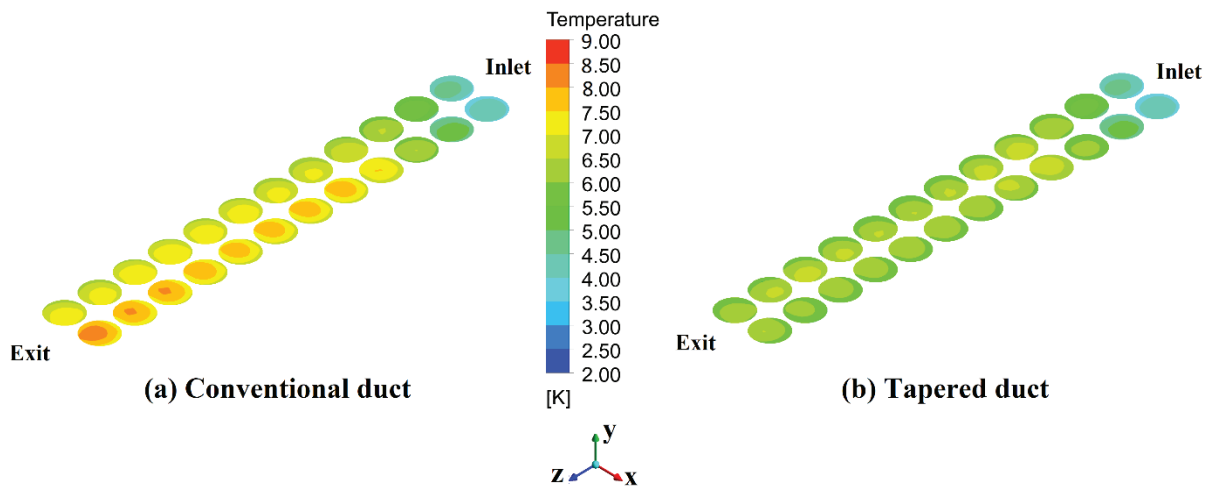


Figure 10. Temperature rise at mid-height of the battery pack for inlet velocity of 1.4 m/s,  $q_{gen} = 50000 \text{ W/m}^3$ , and taper angle = 15°.

Table 1. Improvement in thermal performance of the tapered duct compared to the conventional duct for different values of heat generation rate for inlet velocity of 1 m/s and taper angle = 15°.

Heat generation rate, $q_{gen}$ ( $\text{W/m}^3$ )	Percentage reduction in peak temperature rise	Percentage reduction in temperature difference within the battery pack
30000	11.8	18.8
50000	11.7	18.8
70000	11.8	18.8
90000	11.8	18.8

angle = 15°) is compared in Figure 9. For an inlet velocity of 1.4 m/s, the temperature rise in the cells at mid-height of either duct is provided in Figure 10. The introduction of taper results in improved cooling of cells located near the

outlet, along with a decrease in the peak temperature rise within the cells. The taper results in up to 20.3% reduction in the peak temperature rise within the lithium-ion cells for the inlet velocities considered in the study.

### Heat generation rate

The heat generation rate within the cell was varied to verify the enhancement in thermal performance with the tapered design over a wide range of heat inputs. The heat generation rate varied from 30000 W/m<sup>3</sup> to 90000 W/m<sup>3</sup> for the cell arrangements with the conventional duct and the tapered duct. Table 1 presents the percentage reduction in the peak temperature rise of the cells and the percentage reduction in maximum temperature difference within the battery pack when the tapered duct is used instead of the conventional duct over the range of heat generation rates considered in the study. The significant reduction in peak cell temperature due to the tapered duct is evident over the entire range of heat generation rates. The removal of hotspots in cells located near the exit of the duct results in improved cell-temperature uniformity in the case of the proposed tapered duct design. Thus, with the tapered duct, the percentage reduction in temperature difference within the battery pack is ~18.8% for all cases of heat generation rates considered in the study.

### CONCLUSIONS

The study proposed an effective technique for enhancing the heat transfer performance in air-cooled lithium-ion battery packs by employing converging, tapered airflow ducts. The major conclusions are as follows:

- Compared with the conventional duct, the proposed tapered duct resulted in up to 20% reduction in the peak temperature rise and up to 19% reduction in temperature difference within the battery pack.
- The improvement in cooling performance of the tapered duct is due to the elimination of hotspots on cells near the exit, owing to increased airflow velocity along the tapered duct from the inlet to the exit.
- With an increase in taper angle, the location of peak cell temperature shifts from the outlet region to the central region of the battery pack. This is because, for higher taper angles, the larger flow velocities downstream increase turbulence and local heat transfer near the duct outlet.
- The improved cooling performance of the tapered duct was evident over the entire range of flow velocities and heat generation rates considered in the study.

The proposed method can be used in air-cooled battery packs of electric vehicles, where reduction in peak temperature and improvement in thermal uniformity are critical for the safe and reliable operation of the batteries. However, in electric vehicle applications, constraints regarding weight, space, and cost must be considered when introducing the tapered duct. Furthermore, the optimum taper angle could vary with the number of cells and dimensions of the battery pack. These aspects could be investigated in future studies.

### NOMENCLATURE

$c$	specific heat capacity (J/kgK)
$D$	diameter of the lithium-ion cell (m)
$H$	height of the duct inlet (m)
$k$	thermal conductivity of cell material (W/mK)
$L$	length of the duct (m)
$p$	pressure (Pa)
$q_{gen}$	heat generation rate within the cell (W/m <sup>3</sup> )
$Re$	Reynolds number
$T$	temperature (K)
$U$	duct inlet velocity (m/s)
$\vec{V}$	velocity (m/s)
$W$	width of the duct inlet (m)
$x, y, z$	Cartesian coordinates

#### Greek symbols

$\rho$	density (kg/m <sup>3</sup> )
$\mu$	absolute viscosity of air (kg/ms)

#### Subscripts

<i>cell</i>	cell material
<i>air</i>	air

### AUTHORSHIP CONTRIBUTIONS

Authors equally contributed to this work.

### DATA AVAILABILITY STATEMENT

The authors confirm that the data that supports the findings of this study are available within the article. Raw data that support the finding of this study are available from the corresponding author, upon reasonable request.

### CONFLICT OF INTEREST

The author declared no potential conflicts of interest with respect to the research, authorship, and/or publication of this article.

### ETHICS

There are no ethical issues with the publication of this manuscript.

### REFERENCES

- [1] Rao Z, Wang S. A review of power battery thermal energy management. *Renew Sust Energ Rev* 2011;15:4554–4571. [\[CrossRef\]](#)
- [2] Na X, Kang H, Wang T, Wang Y. Reverse layered air flow for Li-ion battery thermal management. *Appl Therm Eng* 2018;143:257–262. [\[CrossRef\]](#)
- [3] Ma S, Jiang M, Tao P, Song C, Wu J, Wang J, Deng T, Shang W. Temperature effect and thermal impact in lithium-ion batteries: A review. *Prog Nat Sci: Mater Int* 2018;28:653–666. [\[CrossRef\]](#)

- [4] Panchal S, Mathewson S, Fraser R, Culham R, Fowler M. Measurement of temperature gradient ( $dT/dy$ ) and temperature response ( $dT/dt$ ) of a prismatic lithium-ion pouch cell with  $\text{LiFePO}_4$  cathode material. SAE Tech Pap 2017. [CrossRef]
- [5] Thakur AK, Prabakaran R, Elkadeem MR, Sharshir SW, Arıcı M, Wang C, et al. A state of art review and future viewpoint on advance cooling techniques for Lithium-ion battery system of electric vehicles. J Energy Storage 2020;32:101771. [CrossRef]
- [6] Wang T, Tseng KJ, Zhao J. Development of efficient air-cooling strategies for lithium-ion battery module based on empirical heat source model. Appl Therm Eng 2015;90:521–529. [CrossRef]
- [7] Chen D, Jiang J, Kim GH, Yang C, Pesaran A. Comparison of different cooling methods for lithium ion battery cells. Appl Therm Eng 2016;94:846–854. [CrossRef]
- [8] Yu K, Yang X, Cheng Y, Li C. Thermal analysis and two-directional air flow thermal management for lithium-ion battery pack. J Power Sources 2014;270:193–200. [CrossRef]
- [9] Mahamud R, Park C. Reciprocating air flow for Li-ion battery thermal management to improve temperature uniformity. J Power Sources 2011;196:5685–5696. [CrossRef]
- [10] Li X, Zhao J, Yuan J, Duan J, Liang C. Simulation and analysis of air cooling configurations for a lithium-ion battery pack. J Energy Storage 2021;35:102270. [CrossRef]
- [11] Zhang SB, He X, Long NC, Shen YJ, Gao Q. Improving the air-cooling performance for lithium-ion battery packs by changing the air flow pattern. Appl Therm Eng 2023;221:119825. [CrossRef]
- [12] Wang N, Li C, Li W, Huang M, Qi D. Effect analysis on performance enhancement of a novel air cooling battery thermal management system with spoilers. Appl Therm Eng 2021;192:116932. [CrossRef]
- [13] Ibrahim M, Saeed T, El-Shorbagy MA, Nofal TA, Aamir N. Study of pressure drop and heat transfer in cooling of lithium-ion battery with rhombic arrangement with two different outlets and different inlet dimensions. J Energy Storage 2022;50:104255. [CrossRef]
- [14] Park H. A design of air flow configuration for cooling lithium ion battery in hybrid electric vehicles. J Power Sources 2013;239:30–36. [CrossRef]
- [15] Zhang J, Kang H, Wu K, Li J, Wang Y. The impact of enclosure and boundary conditions with a wedge-shaped path and air cooling for battery thermal management in electric vehicles. Int J Energy Res 2018;42:4054–4069. [CrossRef]
- [16] Saw LH, Ye Y, Tay AA, Chong WT, Kuan SH, Yew MC. Computational fluid dynamic and thermal analysis of Lithium-ion battery pack with air cooling. Appl Energy 2016;177:783–792. [CrossRef]
- [17] Lu Z, Meng XZ, Wei LC, Hu WY, Zhang LY, Jin LW. Thermal management of densely-packed EV battery with forced air cooling strategies. Energy Procedia 2016;88:682–688. [CrossRef]
- [18] Xu XM, He R. Research on the heat dissipation performance of battery pack based on forced air cooling. J Power Sources 2013;240:33–41. [CrossRef]
- [19] Zhou H, Zhou F, Xu L, Kong J. Thermal performance of cylindrical Lithium-ion battery thermal management system based on air distribution pipe. Int J Heat Mass Transf 2019;131:984–998. [CrossRef]
- [20] Yang T, Yang N, Zhang X, Li G. Investigation of the thermal performance of axial-flow air cooling for the lithium-ion battery pack. Int J Therm Sci 2016;108:132–144. [CrossRef]
- [21] Fan Y, Bao Y, Ling C, Chu Y, Tan X, Yang S. Experimental study on the thermal management performance of air cooling for high energy density cylindrical lithium-ion batteries. Appl Therm Engineer 2019;155:96–109. [CrossRef]
- [22] Singh LK, Gupta AK, Sharma AK. Hybrid thermal management system for a lithium-ion battery module: Effect of cell arrangement, discharge rate, phase change material thickness and air velocity. J Energy Storage 2022;52:104907. [CrossRef]
- [23] Li F, Ibrahim M, Saeed T, El-Refaey AM, Fagiry MA, Elkhadher BA. Numerical simulation of air outlet spacing change in thermal management lithium-ion battery pack with triangular arrangement for use in electric vehicles. J Energy Storage 2022;49:104117. [CrossRef]
- [24] Alharbi KA, Smaism GF, Sajadi SM, Fagiry MA, Aybar HŞ, Elkhatib SE. Numerical study of lozenge, triangular and rectangular arrangements of lithium-ion batteries in their thermal management in a cooled-air cooling system. J Energy Storage 2022;52:104786. [CrossRef]
- [25] Abusorrah AM, Mebarek-Oudina F, Ahmadian A, Baleanu D. Modeling of a MED-TVC desalination system by considering the effects of nanoparticles: energetic and exergetic analysis. J Therm Anal Calorim 2021;144:2675–2687. [CrossRef]
- [26] Gourari S, Mebarek-Oudina F, Makinde OD, Rabhi M. Numerical investigation of Gas-Liquid Two-Phase flows in a cylindrical channel. Defect Diffus Forum 2021;409:39–48. [CrossRef]
- [27] Al-Turki YA, Mebarek-Oudina F, Ahmadian A, Baleanu D. Flat sheet direct contact membrane distillation desalination system using temperature-dependent correlations: thermal efficiency via a multi-parameter sensitivity analysis based on Monte Carlo method. J Therm Anal Calorim 2021;144:2641–2652. [CrossRef]
- [28] Hai T, Abidi A, Abed AM, Zhou J, Malekshah EH, Aybar HŞ. Three-dimensional numerical study of the effect of an air-cooled system on thermal

- management of a cylindrical lithium-ion battery pack with two different arrangements of battery cells. *J Power Sources* 2022;550:232117. [CrossRef]
- [29] Jiaqiang E, Yue M, Chen J, Zhu H, Deng Y, Zhu Y, et al. Effects of the different air cooling strategies on cooling performance of a lithium-ion battery module with baffle. *Appl Therm Eng* 2018;144:231–241. [CrossRef]
- [30] Zhang F, Lin A, Wang P, Liu P. Optimization design of a parallel air-cooled battery thermal management system with spoilers. *Appl Therm Eng* 2021;182:116062. [CrossRef]
- [31] Yang W, Zhou F, Zhou H, Liu Y. Thermal performance of axial air cooling system with bionic surface structure for cylindrical lithium-ion battery module. *Int J Heat Mass Transf* 2020;161:120307. [CrossRef]
- [32] Mansir IB, Sinaga N, Farouk N, Aljaghtam M, Diyoke C, Nguyen DD. Numerical simulation of dimensions and arrangement of triangular fins mounted on cylindrical lithium-ion batteries in passive thermal management. *J Energy Storage* 2022;50:104392. [CrossRef]
- [33] Sharma DK, Prabhakar A. A review on air cooled and air centric hybrid thermal management techniques for Li-ion battery packs in electric vehicles. *J Energy Storage* 2021;41:102885. [CrossRef]
- [34] Tang Z, Gao Q, Li J, Cheng J. Numerical analysis of temperature uniformity of liquid cooling based battery module with incremental heat transfer area. *J Therm Sci Eng Appl* 2020;12:051006. [CrossRef]
- [35] Kumar B, Mittal S. Prediction of the critical Reynolds number for flow past a circular cylinder. *Comput Methods Appl Mech Eng* 2006;195:6046–6058. [CrossRef]
- [36] Standard k-epsilon Model. Available at: <https://www.afs.enea.it/project/neptunius/docs/fluent/html/th/node58.htm>. Accessed March 10, 2022.
- [37] ANSYS FLUENT User's Guide - Judging Convergence. Available at: <https://www.afs.enea.it/project/neptunius/docs/fluent/html/ug/node833.htm>. Accessed March 10, 2022.
- [38] Stanescu G, Fowler AJ, Bejan A. The optimal spacing of cylinders in free-stream cross-flow forced convection. *Int J Heat Mass Transf* 1996;39:311–317. [CrossRef]